A Supplementary material LHCb-PAPER-2017-046

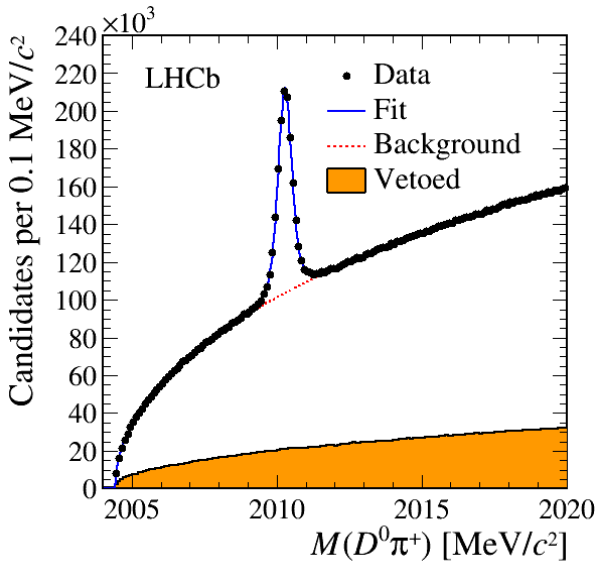

Figure 4: Time-integrated $M(D^0\pi_s^+)$ distribution, with fit projection overlaid, for the WS candidates. The distribution of the WS candidates that are vetoed by the matching requirement of the corresponding D^0 with a RS candidate is overlaid in orange.

Table 1: Measured values of $A_{K\pi} = [\epsilon(K^+\pi^-) - \epsilon(K^-\pi^+)]/[\epsilon(K^+\pi^-) + \epsilon(K^-\pi^+)]$ for each data-taking period, integrated over the kinematic properties of the reconstructed decays.

Data sample	$A_{K\pi}$ [%]
2011	1.10 ± 0.20
2012	1.11 ± 0.13
2015	0.65 ± 0.23
2016	0.98 ± 0.10

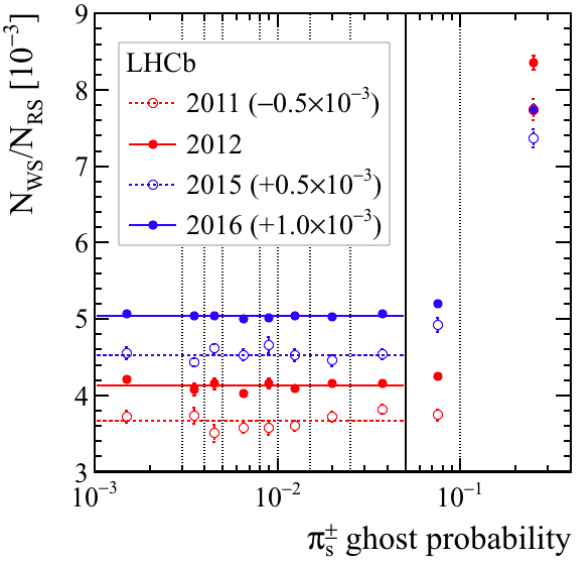

Figure 5: Time-integrated WS-to-RS ratio as a function of the probability for spurious $\pi_s^{\pm}$ reconstruction ("ghost probability") as determined by the discriminant [1], separately for data-taking periods. The candidates meet all the final selection criteria except the ghost probability requirement. The dashed vertical lines indicate the bin boundaries and the solid vertical line indicates the upper threshold used in the analysis. The horizontal lines show the results of fits to uniform distributions in the region below the threshold, which yield χ^2 equal to (2011) 12.8, (2012) 9.3, (2015) 7.7 and (2016) 3.7 for 7 degrees of freedom.

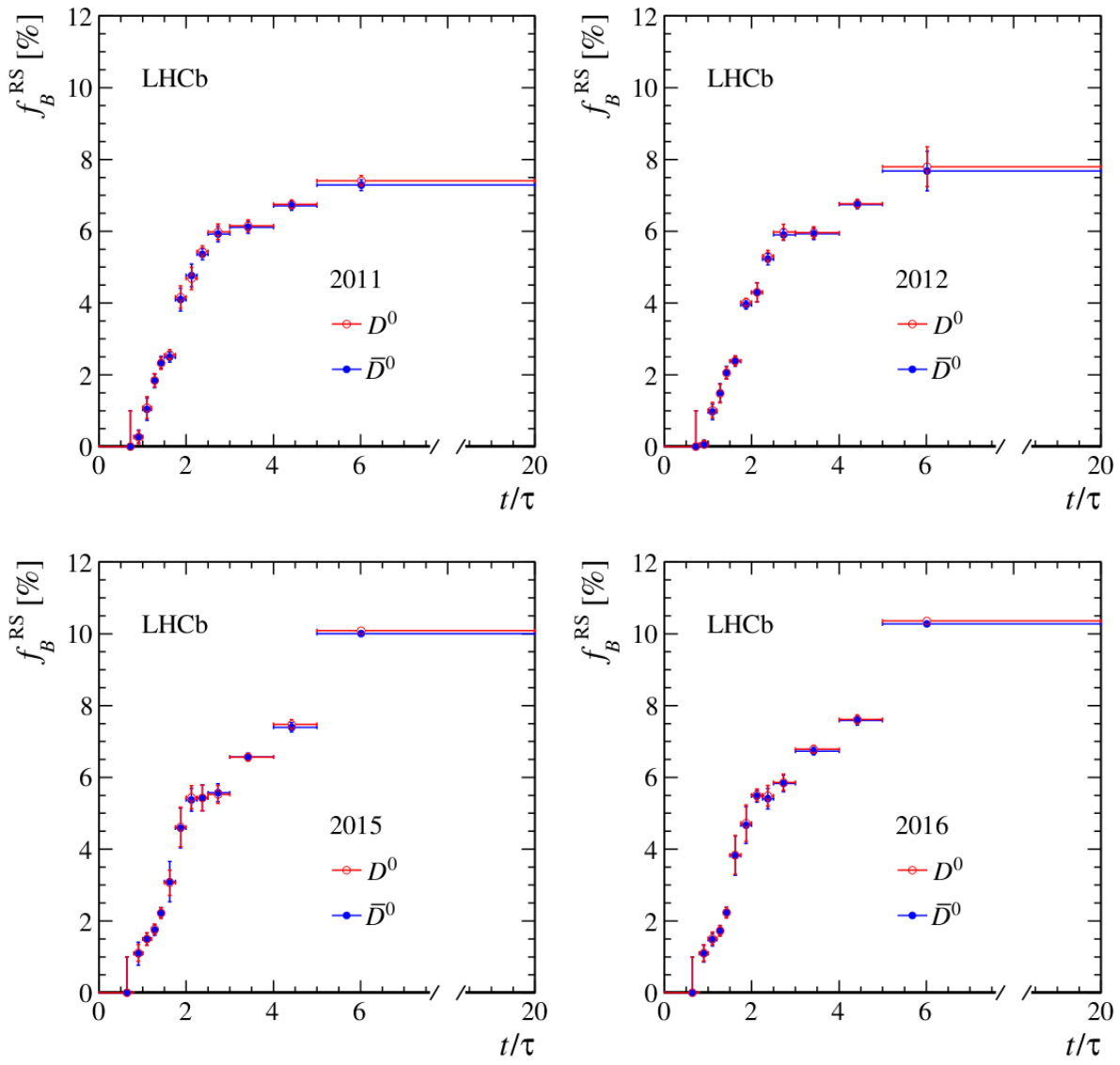

Figure 6: Decay-time evolution, in units of D^0 lifetime, of the contamination from secondary D decays in the RS sample, $f_B^{\rm RS}$, for (top-left) 2011, (top-right) 2012, (bottom-left) 2015, (bottom-right) 2016 data and separately for (open red dots) D^0 and (closed blue dots) $\overline{D}^0$ candidates. The uncertainties are correlated between D^0 and $\overline{D}^0$ decays.

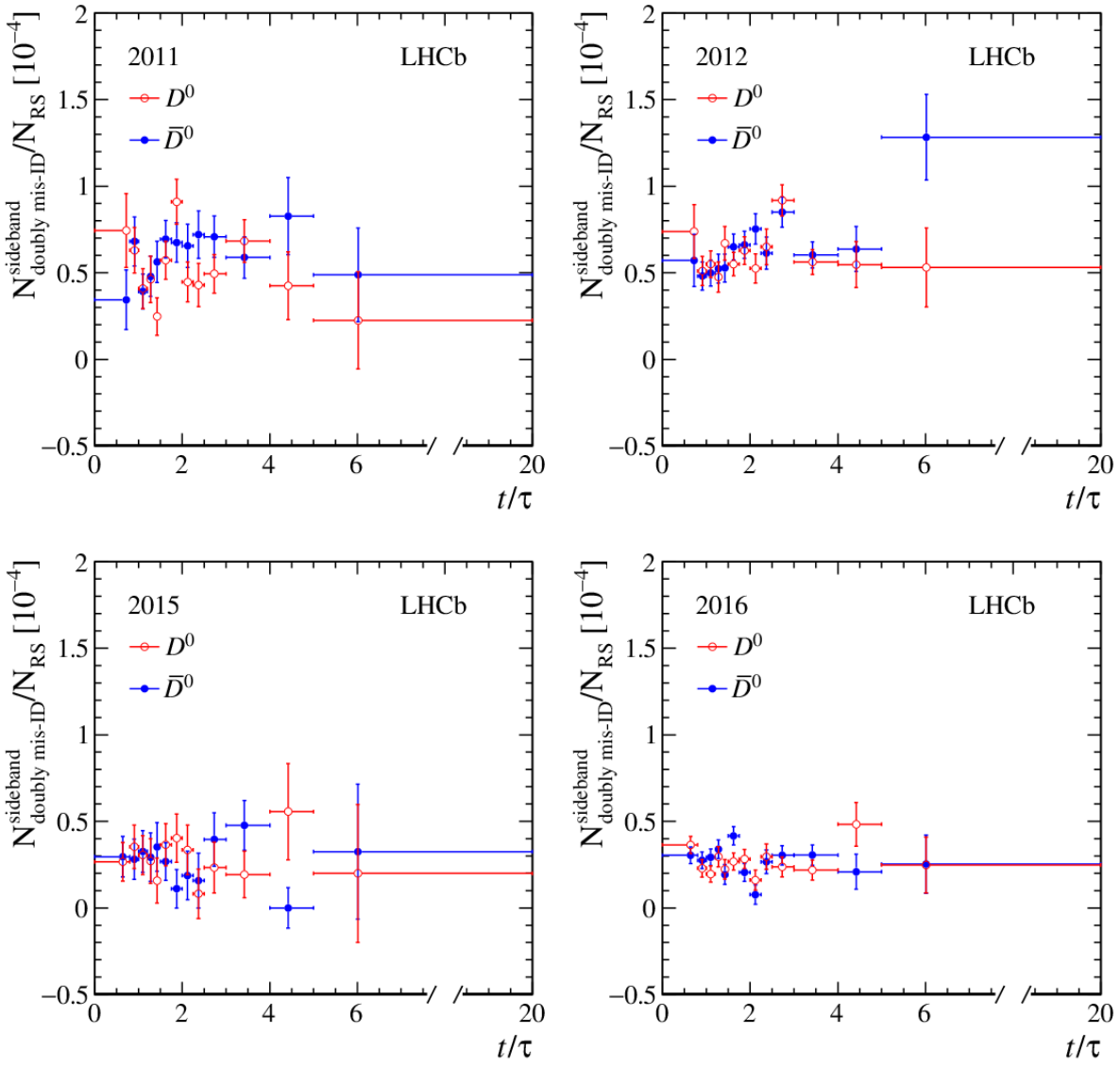

Figure 7: Decay-time evolution, in units of D^0 lifetime, of the contamination from doubly misidentified RS candidates normalized to the RS signal yield for (top-left) 2011, (top-right) 2012, (bottom-left) 2015, (bottom-right) 2016 data and separately for (open red dots) D^0 and (closed blue dots) $\overline{D}^0$ candidates. The 2011–2012 (2015–2016) fractions are multiplied by 0.43 ± 0.06 (0.39 ± 0.11) to be extrapolated in the signal region.

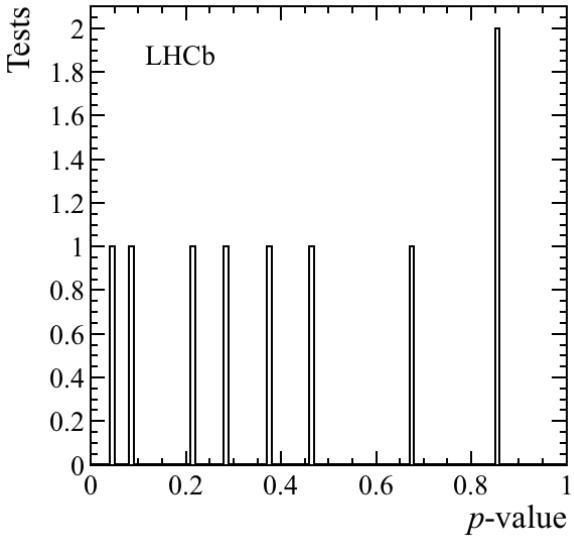

Figure 8: Distribution of the p-values observed in several compatibility checks performed by repeating the fit in which CP violation is allowed in statistically independent subsets chosen according to criteria likely to reveal biases from specific instrumental effects. These criteria include the data-taking year (2011–2012 or 2015–2016), the magnet field orientation, the number of primary vertices in the event, the candidate multiplicity per event, the trigger category, the D^0 laboratory momentum and impact-parameter χ^2 with respect to the primary vertex, and the per-candidate probability to reconstruct a spurious soft pion.

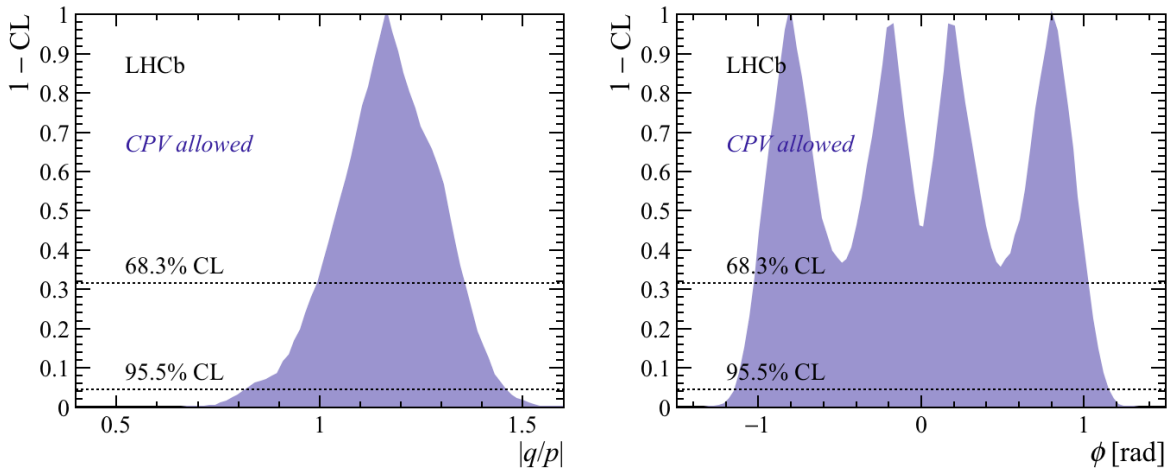

Figure 9: Graphs showing $1-\mathrm{CL}$ versus (left) the magnitude of the ratio of the mixing parameters $|q/p|$ and (right) the CP-violating mixing phase ϕ, as derived from the results of the fit in which CP violation is allowed.

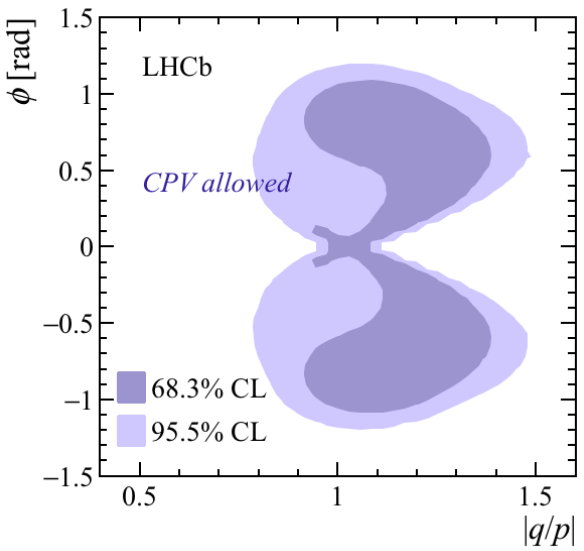

Figure 10: Confidence level regions in the plane $(|q/p|, \phi)$, as derived from the results of the fit in which *CP* violation is allowed. See the caption of the previous figure for definitions of the symbols.

Table 2: Summary of systematic uncertainties.

No CP violation			
Source	R_D $[10^{-3}]$	y' $[10^{-3}]$	x'^2 $[10^{-3}]$
Instrumental asymm.	< 0.001	< 0.01	< 0.001
Peaking background	± 0.003	± 0.04	± 0.002
Secondary D decays	± 0.010	± 0.21	± 0.011
Ghost soft pions	± 0.008	± 0.15	± 0.008
Total syst. uncertainty	± 0.014	± 0.27	± 0.014
Statistical uncertainty	± 0.028	± 0.45	± 0.023

No direct CP violation					
Source	R_D $[10^{-3}]$	y'^+ $[10^{-3}]$	y'^- $[10^{-3}]$	x'^{2+} $[10^{-3}]$	x'^{2-} $[10^{-3}]$
Instrumental asymm.	< 0.001	± 0.08	± 0.08	± 0.003	± 0.004
Peaking background	± 0.003	± 0.04	± 0.04	± 0.002	± 0.002
Secondary D decays	± 0.010	± 0.21	± 0.21	± 0.011	± 0.012
Ghost soft pions	± 0.008	± 0.16	± 0.16	± 0.009	± 0.009
Total syst. uncertainty	± 0.014	± 0.29	± 0.29	± 0.016	± 0.016
Statistical uncertainty	± 0.028	± 0.48	± 0.48	± 0.026	± 0.026

Direct and indirect CP violation						
Source	R_D^+ $[10^{-3}]$	R_D^- $[10^{-3}]$	y'^+ $[10^{-3}]$	y'^- $[10^{-3}]$	x'^{2+} $[10^{-3}]$	x'^{2-} $[10^{-3}]$
Instrumental asymm.	± 0.006	± 0.006	± 0.04	± 0.03	± 0.002	± 0.001
Peaking background	± 0.003	± 0.003	± 0.04	± 0.04	± 0.002	± 0.002
Secondary D decays	± 0.014	± 0.014	± 0.29	± 0.29	± 0.015	± 0.015
Ghost soft pions	± 0.012	± 0.012	± 0.21	± 0.21	± 0.011	± 0.011
Total syst. uncertainty	± 0.020	± 0.020	± 0.38	± 0.38	± 0.019	± 0.020
Statistical uncertainty	± 0.040	± 0.040	± 0.64	± 0.64	± 0.032	± 0.033

References

[1] M. Stahl, *Machine learning and parallelism in the reconstruction of LHCb and its upgrade*, in *22nd International Conference on Computing in High Energy and Nuclear Physics (CHEP 2016) San Francisco, CA, October 14-16, 2016*, 2017. arXiv:1710.08947.